SCIENTIFIC REPORTS

OPEN

SUBJECT AREAS:
SUPERCONDUCTING DEVICES
SUPERCONDUCTING PROPERTIES AND MATERIALS

Received
4 November 2013

Accepted
17 February 2014

Published
1 April 2014

Correspondence and requests for materials should be addressed to B.J. (bjanko@nd.edu)

Quantum rotor in nanostructured superconductors

Shi-Hsin Lin[1,2], M. V. Milošević[2], L. Covaci[2], B. Jankó[1,3] & F. M. Peeters[2]

[1]Department of Physics, University of Notre Dame, Notre Dame, Indiana 46556, [2]Departement Fysica, Universiteit Antwerpen, Groenenborgerlaan 171, B-2020 Antwerpen, Belgium, [3]Materials Science Division, Argonne National Laboratory, Argonne, Illinois 60439.

Despite its apparent simplicity, the idealized model of a particle constrained to move on a circle has intriguing dynamic properties and immediate experimental relevance. While a rotor is rather easy to set up classically, the quantum regime is harder to realize and investigate. Here we demonstrate that the quantum dynamics of quasiparticles in certain classes of nanostructured superconductors can be mapped onto a quantum rotor. Furthermore, we provide a straightforward experimental procedure to convert this nanoscale superconducting rotor into a regular or inverted quantum pendulum with tunable gravitational field, inertia, and drive. We detail how these novel states can be detected via scanning tunneling spectroscopy. The proposed experiments will provide insights into quantum dynamics and quantum chaos.

The classical rotor, a macroscopic particle of mass m confined to a ring, is one of the most studied system in classical mechanics. In a gravitational field the rotor becomes a pendulum with its stable equilibrium at the bottom. Counter-intuitively, the pendulum can also be stabilized at the top by subjecting the pivot to an appropriate drive[1], in a state referred to as an inverted pendulum. Further interest in classical rotors arose from the fact that if one applies periodic kicks to the pendulum, its dynamics becomes chaotic. In contrast to classical rotors, quantum rotors are harder to realize[2]. However, with quantum effects coming into play, quantum rotors furnish even more abundant phenomena than their classical counterparts. For example, the quantum kicked rotor[3] is one of the most featured models of quantum chaos[4] and has various applications[5–9].

Here we show how a quantum rotor can be obtained in nanostructured superconductors. The idea is to trap quasiparticle excitations in a ring-shaped confinement, i.e. a Mexican hat potential, where quasiparticles can form Andreev bound states[10]. The desired potential can be achieved in e.g. annular S-N-S junction [see Fig. 1(a)], a superconducting film with a ring-shaped surface etch ["blind" ring[11]; see Fig. 1(b)], or under a perpendicularly magnetized ferromagnetic disk [Fig. 1(c)] where screening currents suppress the superconducting order parameter mostly within a ring right under the edge of the disk[12,13]. Very recently, it became possible to "draw" the suppression of superconductivity practically at will by locally applying electric field in a ferroelectric/superconductor (FE/SC) bilayer via scanning (AFM) tip [see in Fig. 1(d) and Ref. 14 for details]. On the other hand, to harbor the Andreev bound states, the ring region should preferably be in the clean limit. As discussed later in this manuscript, favorable conditions for experimental detection of the rotor states include: (1) a wide enough ring region, in the order of several coherence lengths, and (2) a sufficiently large ring radius when compared to the ring width, so that the tunneling through the central potential hill is suppressed. Thus, for conventional superconductors such as Pb or Nb, if a ring is fabricated with its width greater than the e-beam lithography resolution (on the order of several tens of nanometers), the ring radius would be on the order of several hundreds of nanometers. It would not be trivial to make these conventional superconductors with such long mean free paths, although recent experiments by the Roditchev lab[15] show that several monolayers of Pb, when deposited onto a Si substrate, become crystalline and exhibit longer mean free paths than bulk Pb. In this respect, graphene-superconductor hybrid is ideal for the realization of our proposal[16–18]. Indeed, superconductor can be nanostructured with a periodic array of ring perforations (using e.g. e-beam lithography) and covered with a graphene flake[see Fig. 1(e)], so that graphene harbors proximity-induced superconductivity with normal regions above the rings. In such a case, the high crystal quality of graphene and therefore the long mean free path ($\sim\mu$m) would guarantee the appearance of the quantum rotor and facilitate its observation. Notably, this would be the very first realization of a superconducting quantum rotor in real space, different from the ones realized in Josephson junctions using the superconducting U(1) phase space[19,20].

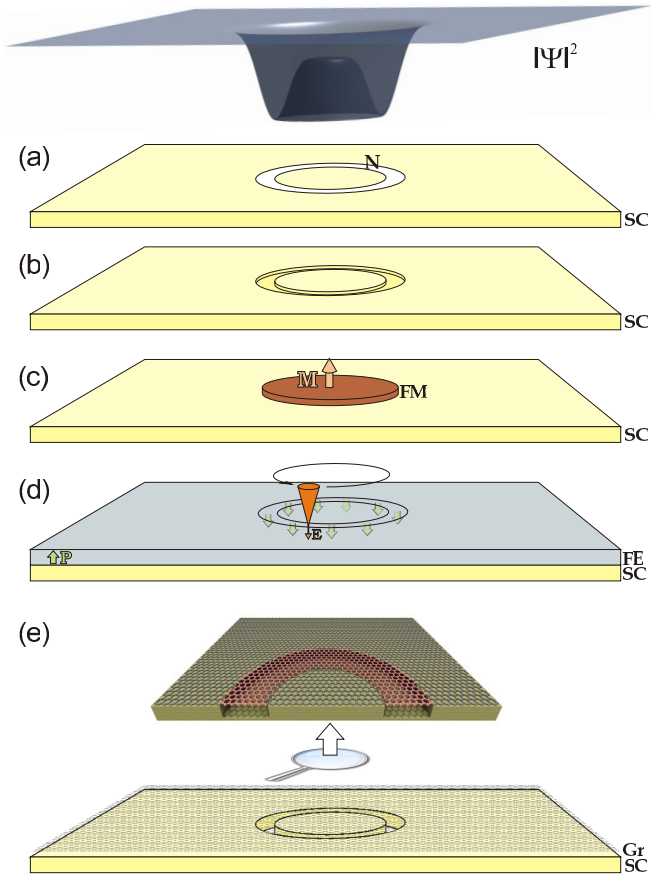

Figure 1 | The 'Mexican hat' order parameter profile required by a superconducting rotor state, realizable e.g. in a superconducting (SC) film with (a) embedded normal-metal ring (annular S-N-S junction), (b) etched "blind" ring on the surface, (c) a ferromagnetic (FM) dot on top with out-of-plane magnetization (M), or (d) ferroelectric (FE) film on top with ring-shaped domain of inverted polarization (P), or (e) graphene flake placed on top of a SC film with ring-shaped perforation.

Results

Unusual quasiparticle energy dispersion. In what follows, we focus on the case of strongly depleted order parameter on the ring, typical for systems of Fig. 1(a), (d) and (e). Nevertheless, our findings can be generalized to any other realization of the Mexican hat potential. We begin our theoretical analysis of those bound states with a simplified model - a step-wise superconducting order parameter with radial symmetry $\Delta(r)$, which vanishes between an inner radius R_{in} and outer radius R_{out}, but it is otherwise constant and finite. We solve the Bogoliubov-de Gennes (BdG) equation in cylindrical coordinates, and separate the rapidly varying degrees of freedom from the slow ones[21] by writing the solutions in the form:

$$\begin{bmatrix} u_l \\ v_l \end{bmatrix} = \begin{bmatrix} f_l \\ g_l \end{bmatrix} H_l^{(1)}(k_F r) + c.c., \tag{1}$$

where u_l and v_l are BdG wave functions, k_F is the Fermi wave vector, r is the radial coordinate, $H_l^{(1)}$ is the Hankel function, and f_l, g_l are slowly varying envelope functions. Next, we insert the WKB-approximated asymptotic form of the Hankel function and change variables[22,23] from r to x, defined by $r^2 = x^2 + b^2$. Here b is the WKB turning point $b = \sqrt{l^2 - 1/4}\,/k_F$, and l is the angular momentum quantum number. For large l, the impact parameter is approximately $b \approx l/k_F$. We obtain:

$$\begin{bmatrix} -iv_F\partial_x & \tilde{\Delta}(x) \\ \tilde{\Delta}(x) & iv_F\partial_x \end{bmatrix} \begin{bmatrix} f_l \\ g_l \end{bmatrix} = \varepsilon \begin{bmatrix} f_l \\ g_l \end{bmatrix}, \tag{2}$$

where $\tilde{\Delta}(x) \equiv \Delta(r(x))$. This maps our two dimensional (2D) problem onto a one dimensional (1D) problem. The 1D order parameter is given by

$$\Delta(x) \begin{cases} \Delta_0 & \text{if } |x| < x_{in} \\ 0 & \text{if } x_{in} < |x| < x_{out} \\ \Delta_\infty & \text{if } |x| > x_{out} \end{cases} \tag{3}$$

where $x_{in} = \sqrt{R_{in}^2 - b^2}$ and $x_{out} = \sqrt{R_{out}^2 - b^2}$. In the quasiclassical picture, the quasiparticles move along a chord in the $\hat{x}$ direction. The distance b of the chord from the center of the 2D ring potential is roughly proportional to the l. This is consistent with the classical picture that a particle with higher angular momentum is localized further away from the pivot. Each orbit with different angular momentum is mapped on a chord of different length. As shown in Fig. 2(a), the $l \approx 0$ state ($b \approx 0$) resides in the most narrow well, with two segments separated by the central hill. As the distance b and the angular momentum increases, the chord length of the bound state (or, equivalently, the width of the potential well) also increases. The bound state energy decreases accordingly as long as $b < R_{in}$. Once b reaches R_{in}, the two segments of the chord merge into one wide potential well, causing the energy to drop to a local minimum $\varepsilon(l_0)$, where $l_0 \approx k_F R_{in}$. As b is increased further, the length of the chord shrinks and energy increases again. Therefore, the dispersion $\varepsilon(l)$ must have a local minimum at a non-zero angular momentum. This is non-trivial and contradicts classical intuition: for such a dispersion faster "rotation" does not always correspond to higher energy. Although very different in origin, such a quantum effect was found earlier in the roton dispersion in superfluid ^{4}He[24–27].

The above reasoning for an unusual dispersion relation is further verified by both analytic and numerical solutions using BdG equations. For $l < l_0 \approx k_F R_{in}$ and $\varepsilon \ll \Delta_0 \leq \Delta_\infty$, the quasiparticle dispersion $\varepsilon_n(l)$ can be obtained analytically by matching the solutions at $x = x_{out}, x_{in}, -x_{in}, -x_{out}$, as

$$\varepsilon_n = \frac{v_F\left[2\pi\left(n + \frac{1}{4}\right) + \sin^{-1}(\tanh(2qx_{in}))\right]}{2(x_{out} - x_{in})}. \tag{4}$$

Here $q = \frac{\Delta_0}{\Delta_\infty}\frac{1}{\xi}$, ξ is the coherence length, and v_F is the Fermi velocity. For $l > l_0$, we obtain

$$\varepsilon_n = \frac{v_F}{2x_{out}}\pi\left(n + \frac{1}{2}\right). \tag{5}$$

The energy levels obtained here coincide with Andreev's result[28] for a normal slab in contact with two superconductors. Note that ε_n depends on l through $x_{in}(l)$ and $x_{out}(l)$ [see Fig. 2(c)]: it decreases with l for $l < l_0$ and then increases for $l > l_0$, as in the case of bound states inside a vortex core[22,29]. We confirmed this analytic result numerically by solving BdG with B-splines basis (see Methods) and direct diagonalization, as shown in Fig. 2(c).

Quantum rotor. In a realistic system [cf. Fig. 1(c)] one likely finds a smooth suppression of the order parameter. Nevertheless, $\varepsilon(l)$ still has a local minimum at non-zero angular momentum, as we show in Fig. 3(a) [for $R \equiv (R_{out} + R_{in})/2 = 12.5\xi$]. The low-lying excitations around the dispersion minimum can then be approximated by a quadratic function $\varepsilon(l) \approx \frac{(l - l_0)^2}{2I}$, where l_0 is the angular momentum of the local minimum, and I is the effective inertia. The magnitude of I is consistent with $m_e R^2$, i.e. the inertia

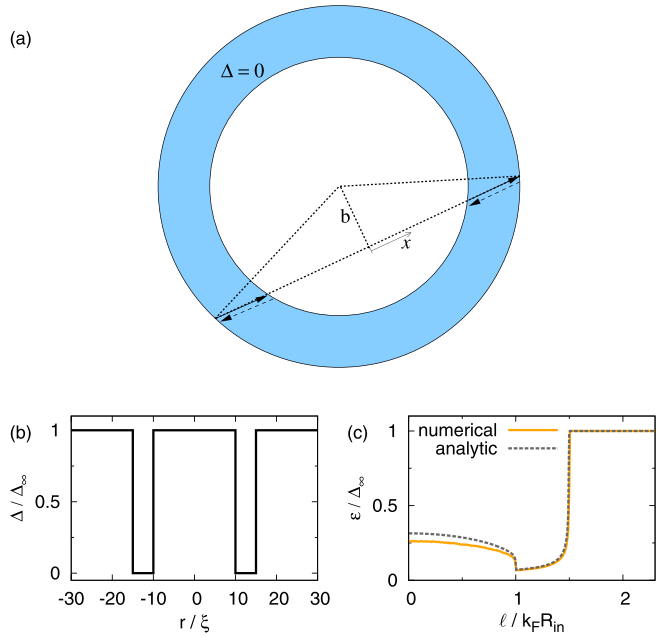

Figure 2 | Andreev bound states and their energy dispersion. (a) Quasiclassical trajectories of the Andreev bound states in the radially step-like order parameter. The bound states are depicted as electrons (solid arrow) being Andreev reflected as a hole (dashed arrow). Here b denotes the distance of the linear reflection path from the center of the 2D potential. (b) Example of a line profile of the order parameter corresponding to panel (a). Panel (c) shows the quasiparticle dispersion of lowest energy states for the step-like potential featured in panel (b).

associated to a quasiparticle confined to move along a circular orbit with radius R. In the present case, the effective inertia obtained for dashed curve in Fig. 3(a) is $I = 7.3 \times 10^{-47}\ kg \cdot m^2$. The effective quasiclassical equation of motion, derived from the Hamiltonian $H = \frac{(l-l_0)^2}{2I}$, is very simple, $\ddot{\theta} = 0$ (θ being the azimuthal angle). This equation describes a free rotor - in our case, a quantum rotor.

To validate the quasiclassical and quadratic approximation, the ring is then required to (1) be equipped with a wide enough width when compared to the coherence length, so that the energy is low enough for those low-lying states, and (2) a large enough radius when compared to the width, in order to suppress tunneling across the central order parameter hill. Notice that the width of the order parameter well in the ferroelectric/superconductor bilayer can be precisely tuned following the method of Ref. 14. This in turn makes the shape of $\varepsilon(l)$ tunable. In other words, one can fine tune externally the effective inertia of the quantum rotor we propose here.

Numerical verification of the rotor state. To confirm these predictions, we solve numerically the BdG equations on a discrete square lattice. Note that in order to compare these results with the quasiclassical limit, we have to consider large systems (e.g. 500 × 500 lattice points). For the size of our nanostructured ring, we take the radius $R = 100a$ and width $W = 30a$, where $a = 1$ is the lattice constant. Here we chose this particular combination of R and W in order to have only one peak for $l = 0$ and a well defined rotor peak for $l = l_0$. If W is larger, multiple overlapping peaks make the analysis cumbersome. The value of the superconducting order parameter is chosen to be $\Delta = 0.1t$, where t is the hopping amplitude, giving a coherence length on the order of the ring width, $\xi \sim 20a$.

We compare in Fig. 3 the local density of states (LDOS) in the middle of planar and ring S-N-S junctions of same width. As seen from the graph, the LDOS is modified only within the superconducting gap due to multiple Andreev reflections at the normal/superconducting interface. For both situations there is a main peak around $E/\Delta = 0.55$ which is mainly given by paths of length W and corresponds to the state with $l = 0$. Interestingly, for the ring geometry an additional peak appears at low energies. This peak is the low-lying state with $l = l_0$ discussed in previous section and is given by the longest chords in the ring. In other words, this peak corresponds exactly to the rotor state.

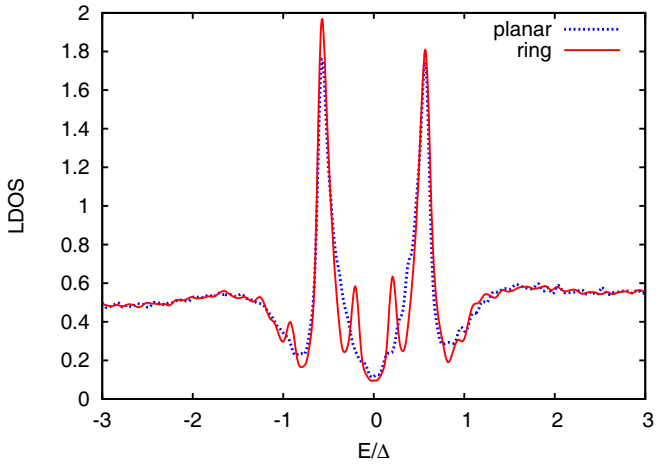

Figure 3 | Rotor peak in full BdG calculations. Local density of states (LDOS) in the middle of a planar S-N-S junction versus one in the middle of a ring junction of same width. The rotor peak at $E/\Delta = 0.088$ is present only in the ring junction.

Discussion

In this Section, we present further implications of the existence of the rotor state, and its manifestations in the presence of applied drive. These effects are interesting in their own right, but also essential for the experimental verification of the rotor state.

Quantum pendulum. It is well-known that superconducting properties can be strongly affected by an electric current. An applied dc current in our system leads to the following effective Hamiltonian for the low-lying states:

$$H = \frac{(l-l_0)^2}{2I} + \mathbf{v_s}\cdot\mathbf{k}, \tag{6}$$

where $\mathbf{k} = (k_F \cos\theta,\ k_F \sin\theta)$ and v_s is the superfluid velocity corresponding to the applied transport current. The equation of motion then exhibits nonlinear dynamics:

$$\ddot{\theta} - \frac{k_F v_s}{I}\sin\theta = 0. \tag{7}$$

For our choice of coordinates, this corresponds to an inverted pendulum. Nevertheless, the "gravitational" force drives the system away from the $\theta = 0$ (up) unstable equilibrium point. To analyze the behavior of this quantum pendulum, we use the effective Hamiltonian in Eq. (6), and show that the thermally averaged zero energy local density of states, $g(r) = \int_{-\infty}^{\infty} \frac{\sum_n |\psi_n(r)|^2 \delta(\epsilon-\epsilon_n)}{4T\cosh^2(\epsilon/2T)} d\epsilon$, has a peak at the bottom position, $\theta = \pi$ [see Fig. 4(c)]. Hence in the presence of an applied dc current our system becomes the quantum analogue of a pendulum in a gravitational field.

Numerical results with applied current. We next show the full numerical solutions of the BdG equations on a discrete lattice in the presence of an external dc current. A supercurrent is applied to the system in y-direction by imposing a phase gradient, $\partial\phi/\partial y$, on the superconducting order parameter.

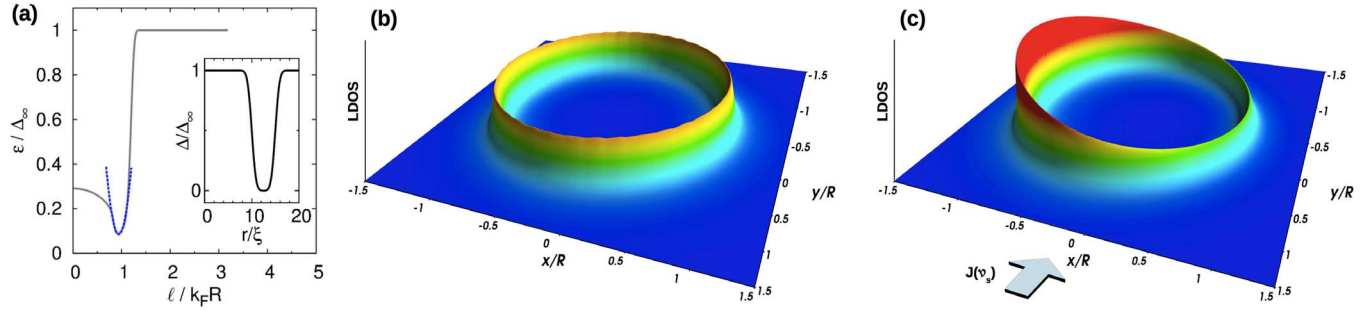

Figure 4 | Manifestation of the quantum rotor in the local density of states. (a) Parabolic approximation (dotted curve) of the energy dispersion [for realistically smoothened order parameter profile shown as inset]. The resulting Hamilton equation of motion corresponds to a rotor. (b) The local density of states (LDOS) calculated for a quantum rotor, for the same parameters as in (a). (c) The calculated LDOS for a quantum pendulum, obtained by injecting a *dc* current in the indicated direction ($v_s = 1.0$ m/s). The finite transport current is effectively equivalent to gravity in the classical pendulum picture.

The dashed line in Fig. 5(a) shows the calculated LDOS(E) for the case without applied current, taken at the bottom position of the ring (at $\theta = \pi$). One notices two main peaks, largest of which corresponds to the state with $l = 0$, whereas the smaller one is the state with $l = l_0$. The solid curve in Fig. 5(a) is calculated at the same place on the ring, but now in the presence of the current along the y-direction. According to Fig. 4, a pendulum state is expected. We indeed observe that the rotor peak is split into pendulum states since there is a phase difference along the chords which contribute to those states. However, because the chiral symmetry is not broken, states with opposite chirality are located at top and bottom locations respectively, as shown in the LDOS map in Fig. 5(b) [for energy corresponding to the lowest energy peak in Fig. 5(a)]. In other words, the two pendulum states at $\phi = \pi$ and $\phi = 0$ are degenerate in energy, but the application of a small perpendicular magnetic field breaks the chiral symmetry and selects only one of them [as shown in Fig. 5(c)]. The LDOS maps for all the energies and other field/current configurations can be found in the Supplementary Material.

Inverted pendulum. Finally we return to Eq. (6) to point out that although the inverted pendulum is unstable, it can be driven to stability by horizontal or vertical pivot motion (cart-pole or Kapitza pendulum, respectively[30]). If the pivot is vibrated with an amplitude A cos ωt, and the frequency ω is much higher than the pendulum's natural frequency ω_N, i.e. more precisely $\omega \gg \frac{R}{A}\omega_N$, where $\omega_N = \sqrt{\hbar k_F v_s / I}$, the effect of the fast pivot motion will be identical to an effective potential[30,31] $V_{eff} = \frac{1}{4} I R^2 a^2 \omega^2 \sin^2\theta$. For such a case, which in a system of Fig. 1(c) [(d)] can be realized by an *ac* in-plane magnetic [electric] field, we calculated the local density of states [see Fig. 6] and indeed observed a peak at the top position $\theta = 0$ of the pendulum, corresponding to the inverted pendulum state. Note, however, that the peak at $\theta = \pi$ for a regular pendulum state remains, which is different from the classical case. Quantum mechanics allows the particle to reside in both potential wells, while classical mechanics forces the particle to choose either bottom or top localization. Finally we note that while the inverted pendulum state is stabilized by a high frequency drive, low-frequency drives are also of interest as they lead to the classically chaotic regime. Therefore, the quantum rotor proposed here is a testbed for further studies of quantum chaology[32]. Applying pulsed current to our device would transform the superconducting rotor into a pendulum with pulsed gravity, i.e. another quantum chaotic system[7–9].

In summary, we provided analytical and numerical results for novel quantum rotor states in nanostructured superconductors. Besides being a remarkable example of a quantum analogue of a classical system, the superconducting rotor (i) can be realized in various superconducting systems, (ii) has a tunable inertia and gravitational field, (iii) can be externally manipulated through effective tilt, pulsed gravity, and pivot oscillations, and (iv) can be converted to a quantum pendulum, inverted pendulum, or be driven to a chaotic regime. Hence this quantum rotor has the potential to provide insights into a variety of phenomena which certainly deserve further experimental and theoretical investigation.

Methods

The Bogoliubov-de Gennes (BdG) equations are used to calculate the spectrum and LDOS throughout this work. The BdG equations provide mean field description of superconductivity and are generalized from the Hartree-Fock equations. We first applied the quasiclassical approximation, which separates the fast oscillation mode with length scale $1/k_F$. It allowed us to discuss physical quantities varying over the superconducting coherence length, and also provided clear physical picture of the quasiclassical trajectories. For the quasiclassical limit, the numerical calculations are done within the B-spline basis[33–35], which is very efficient for inhomogeneous problems such as the one presented here.

We also performed full BdG calculations for a discrete square lattice by using the Chebyshev-BdG method[18,36]. This method can extract relevant physical quantities, for example LDOS, from large systems (here we used a square lattice with 500×500 grid points) and avoid large matrix diagonalization.

In order to describe inhomogeneous s-wave superconductivity we use a real-space tight-binding formulation. The corresponding Hamiltonian written in Nambu spinor form is the following:

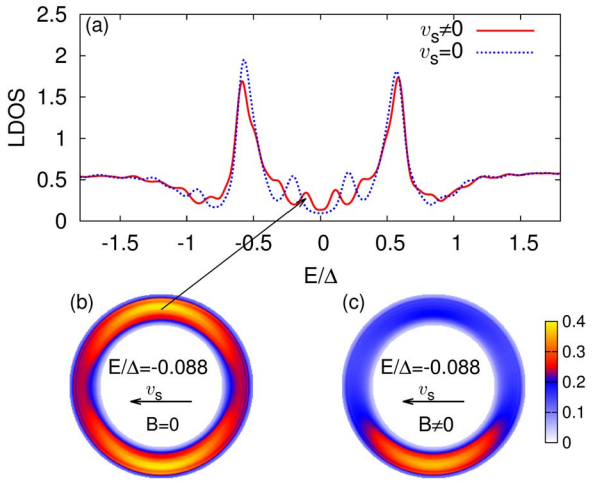

Figure 5 | Realization of the quantum pendulum. (a) Full BdG calculation of the LDOS vs. energy in $\theta = \pi$ location on the ring (of width $W = \xi$ and radius $R = 5\xi$), for the quantum rotor (no current) and pendulum state (with current generated via $\partial\phi/\partial y = 0.0033/a$). The 2D LDOS for a quantum pendulum is shown for $E/\Delta = -0.088$ in the absence (b) and presence (c) of a small perpendicular magnetic field, $\Phi/\Phi_0 = 0.15$.

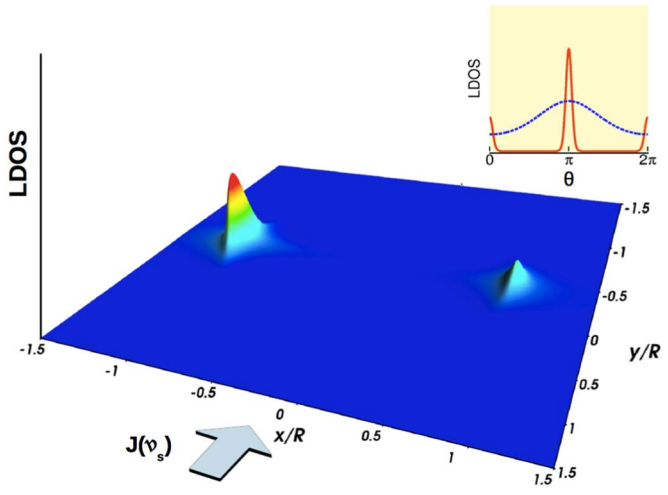

Figure 6 | Pivot oscillations and the inverted pendulum. The localization of a regular and an inverted pendulum, directly observable in STM imaging of LDOS, in the case of the oscillating pivot with amplitude of the oscillation $A = 10$ nm, for high drive frequency $\omega = 50\ \text{GHz} \gg \frac{R}{a}\omega_N \approx 1\ \text{GHz}$. The inset shows LDOS along the circular path of the rotor. The blue/red curve corresponds to the LDOS without/with *ac* drive.

$$\mathcal{H} = \sum_{\langle i,j \rangle} \left(c_{i\uparrow}^{\dagger} \;\; c_{i\downarrow} \right) \hat{\mathcal{H}}_{ij} \begin{pmatrix} c_{j\uparrow} \\ c_{j\downarrow}^{\dagger} \end{pmatrix}, \tag{8}$$

where $\hat{\mathcal{H}}_{ij}$ is a 2×2 matrix:

$$\hat{\mathcal{H}}_{ij} = \begin{pmatrix} -\mu & \Delta_i \\ \Delta_i^{\star} & \mu \end{pmatrix} \delta_{ij} + \begin{pmatrix} -t_{ij} & 0 \\ 0 & t_{ij}^{\star} \end{pmatrix} (1 - \delta_{ij}), \tag{9}$$

where the sum $\langle i, j \rangle$ is over nearest and next-nearest neighbours. The superconducting order parameter, Δ_i, is of s-wave spin-singlet type and is finite outside the ring and and zero inside it. The hopping parameters for nearest neighbor, $t = 2/3t_0$, and next nearest neighbor, $t' = 1/6t_0$ together with the chemical potential $\mu = -2t_0$ are chosen such that the Fermi surface is circular and therefore there is no anisotropy in the Fermi velocity. t_0 is an arbitrary energy unit which is set to 1.

We considered both the influence of an in-plane current and/or an out-of-plane magnetic field on the rotor states. The supercurrent is described by a phase gradient imposed on the superconducting order parameter. The out-of-plane magnetic field is considered to be weak, the flux through a circle of radius R was typically taken to be $\Phi = 0.15\Phi_0$, so that Meissner currents are negligible and a self-consistent solution is not necessary. The magnetic field modifies the hopping parameters in the usual way through the Peierls phase factors, $t_{ij} = |t_{ij}| \exp\left[i \frac{e}{\hbar} \int_i^j \vec{A} d\vec{l} \right]$.

For finding the local density of states inside the ring we use the Chebyshev-BdG method which provides an efficient way of calculating the Gorkov Green function:

$$\bar{G}_{ij}(\omega) = \langle vac | \begin{pmatrix} c_{i\uparrow} \\ c_{j\downarrow}^{\dagger} \end{pmatrix} \hat{G}(\omega) \left(c_{j\uparrow}^{\dagger} \;\; c_{j\downarrow} \right) | vac \rangle, \tag{10}$$

where $\pm\hat{G}(\omega + i\eta) = [\omega + i\eta - \mathcal{H}]^{-1}$, $|vac\rangle$ is the vacuum and the diagonal(normal) and off-diagonal(anomalous) components can be expressed as:

$$\bar{G}_{ij}^{11}(\omega) = \langle c_{i\uparrow} | \hat{G}(\omega) | c_{j\uparrow}^{\dagger} \rangle, \tag{11}$$

$$\bar{G}_{ij}^{12}(\omega) = \langle c_{i\downarrow}^{\dagger} | \hat{G}(\omega) | c_{j\uparrow}^{\dagger} \rangle^{*}. \tag{12}$$

Each of these components can be expanded in terms of Chebyshev polynomials and the moments of the expansion can be efficiently calculated through a recursive procedure:

$$\bar{G}_{ij}^{11(12)}(\tilde{\omega}) = \frac{-2i}{\sqrt{1 - \tilde{\omega}^2}} \sum_{n=0}^{\infty} a_n^{11(12)}(i,j) e^{-i\, n \arccos(\tilde{\omega})}, \tag{13}$$

where the coefficients $a_n^{11}(i,j) = \langle c_{i\uparrow} \mid v_n \rangle$ and $\pm a_n^{12}(i,j) = \left\langle c_{i\downarrow}^{\dagger} \,\middle|\, v_n \right\rangle$ can be obtained by an iterative procedure involving repeated applications of the Hamiltonian on iterative vectors $|v_n\rangle$:

$$|v_{n+1}\rangle = 2\mathcal{H}|v_n\rangle - |v_{n-1}\rangle, \tag{14}$$

where $|v_0\rangle = \left| c_j^{\dagger} \right\rangle$ and $|v_{-1}\rangle = 0$. The local density of states (LDOS) is then:

$$N_i(\omega) = -\frac{1}{\pi} Im\left[\bar{G}_{ii}^{11}(\omega) \right]. \tag{15}$$

We performed the expansions separately for each grid point and further accelerated our calculations by using graphical processing units (GPUs) to perform the sparse matrix - vector multiplications.

1. Blackburn, J. A., Smith, H. J. T. & Gronbech-Jensen, N. Stability and hopf bifurcations in an inverted pendulum. *Am. J. Phys.* **60**, 903–908 (1992).
2. Moore, F. L., Robinson, J. C., Bharucha, C. F., Sundaram, B. & Raizen, M. G. Atom optics realization of the quantum δ-kicked rotor. *Phys. Rev. Lett.* **75**, 4598–4601 (1995).
3. Casati, G., Chirikov, B., Izraelev, F. & Ford, J. [Stochastic behavior of a quantum pendulum under a periodic perturbation] *Stochastic Behavior in Classical and Quantum Hamiltonian Systems*, vol. 93 of *Lecture Notes in Physics* [Casati, G. & Ford, J. (eds.)] [334–352] (Springer Berlin Heidelberg, 1979).
4. Ullmo, D. Many-body physics and quantum chaos. *Rep. Prog. Phys.* **71**, 026001 (2008).
5. Hensinger, W. *et al.* Dynamical tunnelling of ultracold atoms. *NATURE* **412**, 52–55 (2001).
6. Monteiro, T. S., Dando, P. A., Hutchings, N. A. C. & Isherwood, M. R. Proposal for a chaotic ratchet using cold atoms in optical lattices. *Phys. Rev. Lett.* **89**, 194102 (2002).
7. Chabé, J. *et al.* Quantum scaling laws in the onset of dynamical delocalization. *Phys. Rev. Lett.* **97**, 264101 (2006).
8. Chabé, J. *et al.* Experimental observation of the anderson metal-insulator transition with atomic matter waves. *Phys. Rev. Lett.* **101**, 255702 (2008).
9. Lemarié, G. *et al.* Observation of the anderson metal-insulator transition with atomic matter waves: Theory and experiment. *Phys. Rev. A* **80**, 043626 (2009).
10. Kulik, I. Macroscopic quantization and proximity effect in S-N-S junctions. *Sov. Phys. JETP (USSR)* **30**, 944 (1970).
11. Bezryadin, A., Ovchinnikov, Y. N. & Pannetier, B. Nucleation of vortices inside open and blind microholes. *Phys. Rev. B* **53**, 8553–8560 (1996).
12. Milošević, M. V. & Peeters, F. M. Vortex-antivortex nucleation in magnetically nanotextured superconductors: Magnetic-field-driven and thermal scenarios. *Phys. Rev. Lett.* **94**, 227001 (2005).
13. Milošević, M. V. & Peeters, F. M. Interaction between a superconducting vortex and an out-of-plane magnetized ferromagnetic disk: Influence of the magnet geometry. *Phys. Rev. B* **68**, 094510 (2003).
14. Crassous, A. *et al.* Nanoscale electrostatic manipulation of magnetic flux quanta in ferroelectric/superconductor $BiFeO_3/Y\,Ba_2Cu_3O_{7-\delta}$ heterostructures. *Phys. Rev. Lett.* **107**, 247002 (2011).
15. Serrier-Garcia, L. *et al.* Scanning Tunneling Spectroscopy Study of the Proximity Effect in a Disordered Two-Dimensional Metal. *Phys. Rev. Lett.* **110**, 157003 (2013).
16. Heersche, H. B., Jarillo-Herrero, P., Oostinga, J. B., Vandersypen, L. M. K. & Morpurgo, A. F. Bipolar supercurrent in graphene. *NATURE* **446**, 56–59 (2007).
17. Tomori, H. *et al.* Fabrication of ultrashort graphene Josephson junctions. *Physica C* **470**, 1492–1495 (2010).
18. Covaci, L. & Peeters, F. M. Superconducting proximity effect in graphene under inhomogeneous strain. *Phys. Rev. B* **84**, 241401 (2011).
19. Mooij, J. E. *et al.* Josephson persistent-current qubit. *Science* **285**, 1036–1039 (1999).
20. Boukobza, E., Moore, M. G., Cohen, D. & Vardi, A. Nonlinear phase dynamics in a driven bosonic josephson junction. *Phys. Rev. Lett.* **104**, 240402 (2010).
21. Caroli, C., de Gennes, P. G. & Matricon, J. Bound Fermion states on a vortex line in a type II superconductor. *Phys. Letters* **9**, 307–309 (1964).
22. Bardeen, J., Kümmel, R., Jacobs, A. E. & Tewordt, L. Structure of vortex lines in pure superconductors. *Phys. Rev.* **187**, 556–569 (1969).
23. Stone, M. Spectral flow, magnus force, and mutual friction via the geometric optics limit of andreev reflection. *Phys. Rev. B* **54**, 13222–13229 (1996).
24. Landau, L. The theory of superfluidity of helium II. *J. Phys. (USSR)* **5**, 71–90 (1941).
25. Landau, L. On the theory of superfluidity of helium II. *J. Phys. (USSR)* **11**, 91–92 (1947).
26. Feynman, R. P. Application of quantum mechanics to liquid helium. In Gorter, C. J. (ed.) *Progress in Low Temperature Physics*, vol. 1 (Interscience Publishers Inc., New York, 1955).
27. Feynman, R. P. Superfluidity and superconductivity. *Rev. Mod. Phys.* **29**, 205–212 (1957).
28. Andreev, A. Electron spectrum of intermediate state of superconductors. *Sov. Phys. JETP (USSR)* **22**, 455 (1966).

29. Gygi, F. & Schlüter, M. Self-consistent electronic structure of a vortex line in a type-ii superconductor. *Phys. Rev. B* **43**, 7609–7621 (1991).
30. Landau, L. D. & Lifshitz, E. M. *Classical mechanics* (Pergamon, New York, 1958).
31. Cook, R. J., Shankland, D. G. & Wells, A. L. Quantum theory of particle motion in a rapidly oscillating field. *Phys. Rev. A* **31**, 564–567 (1985).
32. Berry, M. Quantum chaology, not quantum chaos. *Phys. Scr.* **40**, 335–336 (1989).
33. Bachau, H., Cormier, E., Decleva, P., Hansen, J. & Martin, F. Applications of B-splines in atomic and molecular physics. *Rep. Prog. Phys.* **64**, 1815–1943 (2001).
34. Sapirstein, J. & Johnson, W. The use of basis splines in theoretical atomic physics. *J. Phys. B: At. Mol. Opt. Phys.* **29**, 5213–5225 (1996).
35. Lin, S.-H., Rappoport, T. G., Berciu, M. & Janko, B. The effect of impurities on spin-polarized Zeeman bound states in dilute magnetic semiconductor-superconductor hybrids. *J. Appl. Phys.* **107**, 034307–034314 (2010).
36. Covaci, L., Peeters, F. M. & Berciu, M. Efficient numerical approach to inhomogeneous superconductivity: The chebyshevbogoliubov de gennes method. *Phys. Rev. Lett.* **105**, 167006 (2010).

Acknowledgments

The work was supported by the Flemish Science Foundation (FWO-Vl), the U. S. Department of Energy, Office of Science, Office of Basic Energy Sciences, under contract W-31-109-Eng-38, and the US National Science Foundation via NSF-NIRT ECS-0609249.

Author contributions

M.V.M. and F.M.P. are experts in the behavior of the superconducting condensate in an inhomogeneous field (such as the stray field of a magnetic dot), whose analysis within the Ginzburg-Landau theory lead to the idea of B.J. of a new Andreev bound state in such a system. S.-H.L. carried out the analytical and numerical solution of quasiclassical BdG calculations to demonstrate the bound state, and developed the simplified Hamiltonian for it. S.-H.L. and M.V.M. then conceived the analogy to the classical rotator in a gravitational field. L.C. performed the full BdG calculations with Chebychev method. All authors contributed to the final scientific statement of the manuscript.

Additional information

Supplementary information accompanies this paper at http://www.nature.com/scientificreports

Competing financial interests: The authors declare no competing financial interests.

How to cite this article: Lin, S.-H., Milošević, M.V., Covaci, L., Jankó, B. & Peeters, F.M. Quantum rotor in nanostructured superconductors. *Sci. Rep.* **4**, 4542; DOI:10.1038/srep04542 (2014).

This work is licensed under a Creative Commons Attribution-NonCommercial-ShareAlike 3.0 Unported License. The images in this article are included in the article's Creative Commons license, unless indicated otherwise in the image credit; if the image is not included under the Creative Commons license, users will need to obtain permission from the license holder in order to reproduce the image. To view a copy of this license, visit http://creativecommons.org/licenses/by-nc-sa/3.0/